ELSEVIER

Journal of Nuclear Materials 275 (1999) 12–18

journal of nuclear materials

www.elsevier.nl/locate/jnucmat

Morphology of UO_2

M. Abramowski [a], R.W. Grimes [a,*], S. Owens [b]

[a] *Department of Materials, Imperial College, Prince Consort Road, London SW7 2BP, UK*
[b] *Research and Technology, BNFL, Springfields works, Salwick, Preston PR4 0XJ, UK*

Received 7 January 1999; accepted 6 April 1999

Abstract

The sintering of UO_2 green pellets is influenced by the morphology of the crystallites. This study predicts equilibrium and growth morphologies of UO_2 crystallites, based on five different interatomic potential models that were derived in order to understand properties of the bulk material. It was found that despite the differences between these models, all result in essentially the same morphologies. The equilibrium morphology of UO_2 is an octahedron, showing only {1 1 1} faces. The growth morphology is a truncated octahedron, exhibiting {1 1 1} and {2 0 0} facets.

PACS: 68.55.Jk; 68.10.Cr; 07.05.Tp; 81.10.Aj

1. Introduction

UO_2 fuel is generally fabricated by pressing powder into green pellets, which are sintered and then assembled into fuel rods [1,2]. Clearly the mechanical properties of the sintered material, in particular the extent and distribution of porosity, are of great concern. Such issues depend critically on the morphology of the crystallites from which the starting powder is composed, since the driving force behind the densification during sintering is the change in free energy brought about by a decrease in the total surface area [3]. Unfortunately, the processes by which UO_2 powder is formed all involve a number of high temperature steps, which are chemically and thermodynamically complex and therefore correspondingly difficult to investigate experimentally. Thus, collaborative data from atomistic scale simulation would be particularly useful.

In this study, calculations based on an ionic model of the UO_2 lattice are used to predict the equilibrium surface (cleavage) energies and attachment (growth) energies of a range of different surfaces, whose Miller-indices (*hkl*) fulfil the condition $h^2 + k^2 + l^2 < 25$. Previous studies on a related material, CeO_2, have shown that higher index surfaces exhibit higher surface and attachment energies, rendering them less important for the crystal morphology [4]. Such a model would also be in agreement with recent experimental results on voids in UO_2 single crystals [5].

2. Methodology

Our calculations are based on a Born description of an ionic lattice [6], where the interatomic forces consist of a long-range Coulomb term and a short-range repulsive term. Thus, the energy U_{ij} between two ions, i and j, is described by

$$U_{ij} = \sum \frac{q_i q_j}{r_{ij}} + A e^{-r_{ij}/\rho} - \frac{C}{r_{ij}^6}, \tag{1}$$

where the short-range component is characterised by three adjustable parameters, A, ρ and C, which together define what is usually termed the 'Buckingham short-range potential'. Since the short-range energy converges to zero quickly, to make the calculations more efficient, this part of the interaction energy is assumed to be zero beyond 1.4 nm.

The polarisability of ions is realised through a shell model, so that each ion is described as a massless

* Corresponding author. Tel.: +4-171 594 6730; fax: +4-171 584 3194; e-mail: r.grimes@ic.ac.uk

0022-3115/99/$ - see front matter
PII: S0022-3115(99)00110-5

spherical shell of charge Y, coupled to a massive core of charge X: the total ion charge is $(X + Y)$. The interaction between the shell and the core is described by the force

$$F = k_2\delta r + \tfrac{1}{6}k_4\delta r^3, \quad (2)$$

where k_2 is a harmonic spring constant and k_4 an anharmonic contribution. Generally, only a k_2 term is used although in some cases, the k_4 term is required to prevent unphysically large core-shell separations. The maximum core-shell separation allowed in this work was 0.5 Å.

In this study we used five different sets of potential and k_2 parameters, each developed earlier [7–10] and summarised in Table 1. The sets referred to as Catlow1 [7], Jackson [8], Grimes [9] and Busker [10] all assume formal charge states so that, for example, the total charge of an oxygen ion $(X + Y) = -2$. For the Catlow2 model [7], the total charges for uranium and oxygen are reduced to 3.84 and −1.93, respectively. Each potential set was derived by fitting to bulk lattice properties: in Table 2, predicted bulk properties are compared to experimental data. As can be seen, in all cases the lattice parameter of UO_2 is reproduced successfully. However, the extent to which other bulk lattice properties are reproduced varies considerably from potential to potential. For example, the activation energy for oxygen migration through the lattice via oxygen vacancies is most successfully calculated with the Catlow1 and Jackson models.

Surface formation energies were calculated using the code 'MARVIN' [11]. In this program, the simulated surface is created by repeating the simulation cell in the two dimensions parallel to the surface. The simulation cell itself consists of several UO_2 cubic unit cells, stacked on top of each other. This stack is divided into two regions: region I and region II. In region I, all ions are relaxed explicitly until they experience zero strain. The ions in region II only contribute to the force field in region I and therefore, remain fixed at the usual crystallographic coordinates. In our calculations, both regions had a depth of 6 unit cells or 3.3 nm. This value was chosen so that if increased further, it had negligible effect on surface energies. It is equal to the region sizes used in the previous study of CeO_2 [4].

We shall calculate two distinctly different types of surface formation energetics, known as surface and attachment energies. The surface energy is defined as the energy required to cleave that surface from a bulk crystal. The most stable surface is the one with the lowest surface energy, i.e. the mode of cleavage which requires the least amount of energy. The attachment energy is the energy released when a growth slice of thickness d_{hkl} is attached to the surface from infinity [12]. It is usually negative, for energy is gained when matter is attached to the crystal face. The most favourable surface from the attachment point of view is that which exhibits the highest (= closest to zero) attachment energy. A high attachment energy means that material tends not to be added to this surface. Thus, material is added preferentially to adjacent surfaces, resulting in the formation of more of this surface. Attachment energies used in this way best model two dimensional layer-by-layer growth of the type investigated extensively using molecular beam epitaxy (see for example [13]) and computer simulation [14]. Attachment energies are less obviously useful to model the growth of rough surfaces [13,14]. Therefore, the present work relates to smooth growth regimes.

The situation is made more complex by the fact that, in an ionic material, there are three types of surfaces, classified by Tasker [15] as follows (see Fig. 1). Type I

Table 1
Spring and Buckingham potential parameters for the five models. In the Catlow2 model, the total charges for U^{4+} and O^{2-} are reduced to 3.84 and −1.93, respectively

Potential	Catlow1 [7]	Catlow2 [7]	Jackson [8]	Grimes [9]	Busker [10]
U^{4+}: k (eV Å^{-2})	103.38	210.02	103.98	98.24	160.0
Y (e)	6.54	7.94	6.54	6.54	−0.1
O^{2-}: k (eV Å^{-2})	292.98	80.21	292.98	296.8	6.3
Y (e)	−4.4	−3.06	−4.4	−4.4	−2.08
O^{2-}–O^{2-}: A (eV)	22764.3	22764.3	20378.0	108.0	9547.96
ρ (Å)	0.149	0.149	0.12537	0.38	0.2192
C (eV Å^6)	112.2	20.37	114.0	56.06	32.0
U^{4+}–O^{2-}: A (eV)	1217.8	1217.44	1217.8	2494.2	1761.775
ρ (Å)	0.3871	0.3747	0.3871	0.34123	0.35642
C (eV Å^6)	0.0	0.0	0.0	40.16	0.0
U^{4+}–U^{4+}: A (eV)	0.0	0.0	0.0	18600.0	0.0
ρ (Å)	0.0	0.0	0.0	0.27468	0.0
C (eV Å^6)	0.0	0.0	0.0	32.64	0.0

Table 2
Bulk properties resulting from the five models used and from experiments

Potential	Catlow1 [7]	Catlow2 [7]	Jackson [8]	Grimes [9]	Busker [10]	Experiment
Lattice constant (Å)	5.450	5.441	5.447	5.461	5.468	5.468
Lattice energy (eV)	−102.97	−94.50	−103.00	−105.56	−104.47	−106.7
ϵ_0	21.26	25.52	21.14	13.26	18.53	21.45
ϵ_∞	5.357	5.197	5.364	5.260	6.203	5.0
Bulk modulus B (10^{11} dyn/cm^2)	22.30	21.15	22.30	27.20	25.85	17.89
Shear modulus S_1 (10^{11} dyn/cm^2)	14.80	16.70	14.70	18.88	20.49	9.01
Shear modulus S_2 (10^{11} dyn/cm^2)	6.52	5.70	6.58	8.86	11.84	5.97
O^{2-} Migration energy (eV)	0.515	0.300	0.522	0.694	0.313	0.51
Total Schottky energy (eV)	9.67	7.03	9.73	13.27	10.56	n.a.
Per defect (eV)	3.22	2.34	3.24	4.42	3.52	n.a.
Total anion Frenkel energy (eV)	4.92	4.92	5.00	6.82	6.36	n.a.
Per defect (eV)	2.46	2.46	2.50	3.41	3.18	n.a.

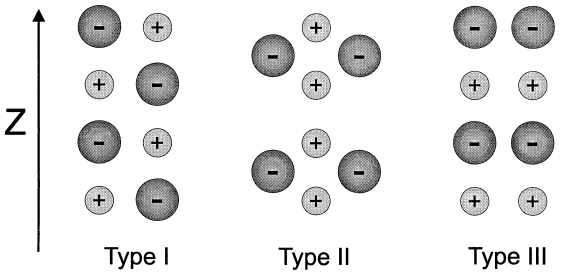

Fig. 1. The three types of surfaces, according to Tasker [15].

surfaces have anions and cations in the same surface and thus can be cut anywhere without creating an electrical dipole moment in the direction of the surface normal. Type II surfaces consist of symmetrically arranged, charged planes of ions. The surface can be cut at specific points without creating a dipole moment. The (1 1 1)-surface of UO_2 is a type II surface. Type III surfaces consist of alternating layers of anions and cations and therefore cannot be terminated without creating an electrical dipole orthogonal to the surface. The (2 0 0)-surface of UO_2 is of this type.

To neutralise the dipole associated with the (2 0 0) surface, half of the layer of ions at the bottom of region II are moved on top of the surface, i.e. above region I. For the (2 0 0) surface of a single cubic UO_2 unit cell, this is possible in three different ways. The first two options are viable if the bottom plane consists of oxygen ions. Half of these can be moved to the top of the surface to create either diagonal (A) or close-packed (B) lines (see Fig. 2). If the bottom plane consists of uranium ions, there is only one way of moving half of them to the top (C). Where used, the respective configuration is indicated in the tables. For higher index surfaces, the oxygen atoms are not distributed in a square pattern. We therefore define configuration A as a defect configuration of second nearest neighbours and configuration B as one of nearest neighbours, with regard to a single unit cell. For surfaces, where the oxygen atoms are distributed in a diamond pattern (such as the (2 2 1) and (3 2 2) surfaces), resulting in six nearest neighbours surrounding each oxygen atom in the plane parallel to the surface, the distances between neighbouring oxygen atoms differing by less than 0.003 nm, configuration A and B are practically equivalent and give very similar surface formation energies.

Both surface and attachment energies were used as the basis for a Wulff construction [16], so that equilibrium and growth crystallite morphologies were predicted. Since we employ five potential models, this results in a total of 10 morphologies. In a Wulff construction, all simulated surfaces are drawn so that the distance from the origin is proportional to the respective surface or attachment energy. Fig. 3 shows a two-dimensional example. The smallest completely enclosed volume represents the equilibrium or growth morphology, depending on which set of energies is used.

In all the calculations described here, the two-dimensional surface repeat unit was constructed within a single conventional cubic unit cell. Clearly, for type III

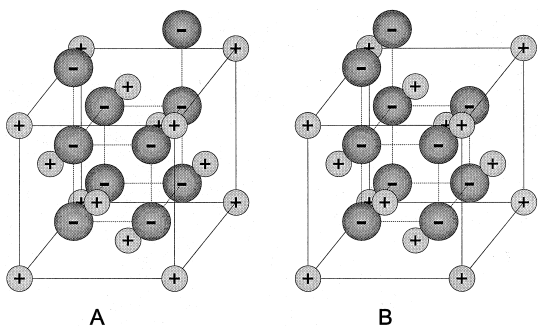

Fig. 2. The two ways of ordering oxygen defects on the (2 0 0) surface of UO_2.

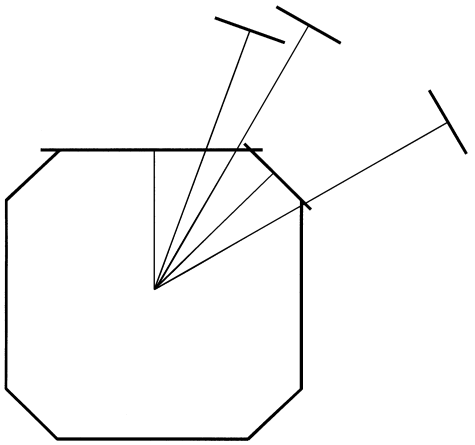

Fig. 3. Wulff construction. The lengths of the surface normals are proportional to the respective surface energies.

surfaces, where it is necessary to introduce a distribution of defects on the surface, repeat units larger than a single unit cell would provide a greater number of potential arrangements of defects. Indeed we have investigated this for the (2 0 0) surface, based on a repeating unit formed from a 2×2 arrangement of single unit cells. This resulted in 105 different ways of arranging oxygen defects alone. However, none of these configuration energies resulted in a significant (i.e. visible) change to either type of predicted morphology. The details of these computationally challenging simulations will be provided in a future communication. However, since they are not significant to the conclusions made in this work, they will not be discussed further.

Since the relaxation algorithm leads to a local minimum and thus may miss the globally smallest surface energy for that surface, some of the surface configurations were pre-relaxed by using one of the other models,

Table 3
Surface energies [J/m^2] for unrelaxed (U) and relaxed (R) UO_2 surfaces

Surface	Cut	Catlow1		Catlow2		Jackson		Grimes		Busker	
		U	R	U	R	U	R	U	R	U	R
1 1 1	0.5	1.60	1.18	1.26	0.89	1.61	1.19	1.83	1.48	1.56	1.27
2 0 0	0.125A	6.13	2.35	5.39	1.43	6.14	2.37	6.49	2.99	6.09	2.81
	0.125B	8.60	2.59	7.85	1.91	8.61	2.61	9.14	3.47	8.74	3.11
	0.375C	10.92	2.66	10.28	1.92	10.93	2.68	11.73	3.84	11.34	3.80
2 1 0	0.125A	5.30	1.93	4.83	1.28	5.31	1.95	5.83	2.57	5.47	2.28 [b]
	0.125B	5.32	1.91	4.84	1.21	5.33	1.93	5.84	2.53	5.49	2.30
	0.375C	13.44	2.80	12.60	1.77	13.47	2.76	15.35	2.87	13.96	2.47
2 1 1	0.25	6.42	1.93	5.87	1.22	6.43	1.95	6.90	2.61	6.56	2.22
2 2 0	0.25	3.30	1.74	2.96	1.28	3.31	1.75	3.72	2.25	3.42	2.00
2 2 1	0.125A	8.15	1.41 [a]	7.46	1.00 [a]	8.16	1.42 [a]	8.62	1.81	8.27	1.58 [a]
	0.125B	2.53	1.40	2.17	0.97	2.54	1.40	2.86	1.80	3.55	1.57
	0.375C	20.50	2.75 [b]	6.13	1.24	6.71	2.43 [b]	7.19	2.56	6.84	2.75 [b]
3 1 0	0.25	10.91	2.56	10.17	1.76	10.93	2.58	11.58	3.25	11.21	3.30
3 1 1	0.75	7.33	2.11	6.78	1.26	7.34	2.13	7.91	2.89	7.56	2.50
3 2 0	0.125A	4.70	1.84	4.27	1.25	4.71	1.85	5.20	2.43	4.87	2.19
	0.125B	9.21	2.21 [b]	8.47	1.44	9.21	2.24	9.80	2.79 [b]	9.49	2.79 [b]
	0.375C	9.19	2.21	8.49	1.65	9.21	2.50 [b]	9.32	3.20 [b]	9.37	2.78
3 2 1	0.5	5.24	2.21	4.76	1.09	5.25	1.76	5.71	2.35	5.37	1.74
3 2 2	0.125A	11.48	1.77 [a]	10.55	1.11	11.50	1.78	11.95	2.38 [a]	11.58	1.99 [b]
	0.125B	21.84	1.78 [a]	20.23	1.16 [a]	21.88	1.79 [b]	22.39	2.37 [a]	21.96	2.00 [a]
	0.375C	8.37	1.55 [a]	7.63	1.01	9.66	1.56 [a]	9.32	2.04	9.76	1.76 [a]
3 3 1	0.5	2.84	1.45	2.48	1.00	2.85	1.46	3.21	1.89	2.90	1.64
3 3 2	0.5	12.71	1.32 [a]	11.70	0.94 [a]	12.73	1.33 [a,b]	13.18	1.68	12.81	1.43 [a]
4 1 0	0.125A	12.92	2.40	12.01	1.44 [a]	12.94	2.40 [a]	13.56	3.12	13.17	2.82 [a,b]
	0.125B	17.63	2.47 [b]	16.42	1.51 [a]	17.65	2.49 [a]	18.30	3.33	17.89	2.58 [b]
	0.375C	17.63	2.54 [a]	16.42	1.63 [a]	18.22	2.56 [a]	18.92	2.76	20.36	2.85 [a]
4 1 1	0.5	11.80	2.38	10.97	1.55 [a]	11.82	2.45	12.43	3.25 [a]	12.05	2.75 [a,c]
4 2 1	0.25A	7.26	2.87	6.67	2.59	7.27	2.38	9.29	3.15	7.44	3.91 [c]
	0.25B	7.26	2.04	6.67	1.30	7.27	2.54	7.80	3.14	7.44	2.30 [c]
	0.5C	7.23	2.08 [b]	6.67	1.30	7.25	2.08	7.88	2.89	7.43	2.09 [b]

[a] Denotes a pre-relaxation performed with a different potential.
[b] Denotes the use of a k_4 parameter which was discarded after preliminary relaxation.
[c] Denotes the use of a k_4 parameter which could not be discarded.

if that yielded a smaller surface energy than using only the pure model. This was possible due to the model dependent dislocations of atoms, especially for the higher index surfaces.

3. Results and discussion

Tables 3 and 4 show the unrelaxed and relaxed surface and attachment energies for the simulated surfaces. The cut is defined as the point at which the unit cell is terminated [4]. We find that, of the methods for dipole neutralisation for the type III (2 0 0) surface, configuration A is the most favourable. The reason for this is that it has the most uniform charge distribution across the surface. In comparison, configuration B places the oxygen atoms closer to each other. Configuration C creates uranium defects, with twice the charge of the oxygen defects, which explains why configuration C is the least favourable way of forming a stable (2 0 0) surface. Similar results were found for CeO_2 [4].

The rationalisation used to explain why configuration A is the one preferred for the (2 0 0) surface does not generally hold for higher index type III surfaces (see Tables 3 and 4). There is a number of reasons for this, which are surface specific. For example, results for the (2 1 0) surface show that A and B type configurations have essentially the same surface energy (see Table 3). The reason is that the distance between surface layer oxygen ions for (2 1 0) A and B configurations is very similar. The same holds true for the (2 2 1) surface. However, the (4 1 0) surface, as the Miller index suggests, is more similar in structure to the (2 0 0) surface and therefore, configuration A is once again distinct from configuration B and thus generally preferred. The (3 2 2) and (4 2 1) surfaces present more of a problem. They seem to show a preference for the type C configuration (i.e. U^{4+} ions on the surface). However, these

Table 4
Attachment energies [eV/molecule] for unrelaxed (U) and relaxed (R) UO_2 surfaces

Surface	Cut	Catlow1		Catlow2		Jackson		Grimes		Busker	
		U	R	U	R	U	R	U	R	U	R
1 1 1	0.5	−2.53	−2.97	−2.02	−2.52	−2.54	−2.98	−2.92	−3.25	−2.51	−3.02
2 0 0	0.125A	−10.60	−4.44	−9.42	−2.89	−10.61	−4.50	−11.38	−5.48	−10.75	−4.92
	0.125B	−14.06	−13.51	−12.90	−13.16	−14.07	−13.53	−15.16	−13.67	−8.85	−13.00
	0.375C	−19.63	−20.07	−18.48	−18.89	−19.63	−20.07	−21.28	−21.76	−20.60	−21.05
2 1 0	0.125A	−11.88	−10.02	−10.93	−8.92	−11.89	−10.04	−13.03	−11.00	−12.42	−10.59
	0.125B	−11.88	−11.10	−10.92	−11.14	−11.89	−11.09	−13.03	−12.03	−12.41	−12.12
	0.375C	−13.55	−21.38	−14.35	−10.04	−13.55	−23.81	−14.31	−19.74	−14.29	−21.24 [b]
2 1 1	0.25	−18.26	−19.86	−16.81	−21.89	−18.27	−19.87	−19.41	−22.32	−18.77	−24.76
2 2 0	0.25	−10.30	−13.58	−9.43	−15.35	−10.31	−13.52	−11.45	−14.02	−10.81	−14.32
2 2 1	0.125A	−29.99	−6.82 [a]	−27.64	−6.15 [a]	−30.00	−6.83	−31.26	−7.53	−30.55	−7.31 [a]
	0.125B	−6.01	−6.81	−5.23	−6.14	−6.02	−6.83	−6.68	−7.53	−6.19	−7.31
	0.375C	−21.12	−27.68 [b]	−19.39	−28.23	−21.41	−30.56 [b]	−22.33	−27.29	−21.89	−28.45 [b]
3 1 0	0.25	−45.75	−39.25	−42.86	−40.95	−45.76	−39.21	−48.05	−33.94	−47.21	−44.24
3 1 1	0.75	−31.56	−39.82	−29.56	−48.09	−31.57	−39.66	−33.66	−40.10	−32.84	−46.55
3 2 0	0.125A	−16.33	−19.55	−15.12	−20.05	−16.33	−19.49	−17.84	−20.57	−17.10	−21.40
	0.125B	−38.87	−37.72 [b]	−36.07	−20.73	−38.86	−37.67	−40.71	−25.76 [b]	−40.03	−25.15 [b]
	0.375C	−37.77	−39.30	−35.01	−13.68	−37.78	−37.30 [b]	−39.35	−46.78 [b]	−38.59	−37.75
3 2 1	0.5	−20.55	−25.00	−18.94	−34.29	−20.57	−24.79	−21.99	−26.37	−21.22	−37.71
3 2 2	0.125A	−55.57	−19.20 [a]	−51.32	−20.46	−55.60	−19.16	−57.11	−20.43 [a]	−56.24	−26.65 [b]
	0.125B	−120.25	−20.82 [b]	−111.56	−25.92 [a]	−120.29	−24.59 [b]	−122.58	−27.02 [a]	−121.51	−26.64 [a]
	0.375C	−40.07	−15.65 [a]	−36.93	−17.06	−42.52	−15.64 [a]	−41.53	−17.11	−43.24	−17.70 [a]
3 3 1	0.5	−9.12	−14.20	−8.13	−15.48	−9.13	−14.14	−10.08	−14.17	−9.40	−14.25
3 3 2	0.5	−72.75	−57.25 [a]	−67.23	−53.97 [a]	−72.78	−57.23 [a,b]	−74.42	−58.87	−73.49	−58.41 [a]
4 1 0	0.125A	−72.66	−43.72	−67.77	−48.90 [a]	−72.68	−42.63 [a]	−75.23	−41.78	−74.24	−49.25 [a,b]
	0.125B	−87.78	−72.23 [b]	−81.93	−63.73 [a]	−87.80	−72.28 [a]	−90.54	−70.75	−89.55	−47.63 [b]
	0.375C	−87.77	−38.32 [a]	−81.91	−36.84 [a]	−87.46	−38.38 [a]	−90.13	−64.00	−91.23	−37.54 [a]
4 1 1	0.5	−57.87	−35.33 [a]	−54.11	−32.55 [a]	−57.88	−35.43 [a]	−60.46	−34.97 [a]	−59.49	−33.56 [a,c]
4 2 1	0.25A	−28.51	−38.42	−27.45	−20.64	−29.47	−30.25	−31.40	−35.97	−29.60	−43.71
	0.25B	−33.62	−30.58	−31.36	−37.48	−29.06	−26.86	−35.62	−33.28	−31.20	−31.45
	0.5C	−31.84	−22.78 [b]	−29.60	−29.63	−31.86	−38.67	−30.56	−38.82	−32.88	−24.10 [b]

[a] Denotes a pre-relaxation performed with a different potential.
[b] Denotes the use of a k_4 parameter which was discarded after preliminary relaxation.
[c] Denotes the use of a k_4 parameter which could not be discarded.

surfaces are not very stable and rearrange considerably so that oxygen ions relax to the surface, forming a rumpled oxygen terminated surface.

The 10 predicted morphologies are presented in Figs. 4 and 5. All five potential models yield similar equilibrium and similar growth morphologies. The predicted equilibrium morphology of UO_2 is dominated by (1 1 1)-surfaces, creating an octahedral crystallite. For the Catlow2 and Busker potential models, higher index surfaces appear, rounding the tips and edges of the crystallite, although in the latter case, the effect of surfaces other than (1 1 1) is hardly perceptible.

The growth morphologies are all predicted to be truncated octahedra with varying amounts of (2 0 0) surfaces apparent. Although the point of truncation differs from model to model, the respective attachment energy ratios are quite similar. This demonstrates the sensitivity of morphologies predicted using a Wulff construction to very small changes in energy ratios.

Figs. 6 and 7 show the relaxed surface energies of the (1 1 *n*) and (0 1 *n*) sets of planes as a function of the misorientation angle, i.e. the angle between the corresponding (1 1 *n*) or (0 1 *n*) plane and the (1 1 0) or (2 0 0) plane, respectively. Figs. 8 and 9 show relaxed

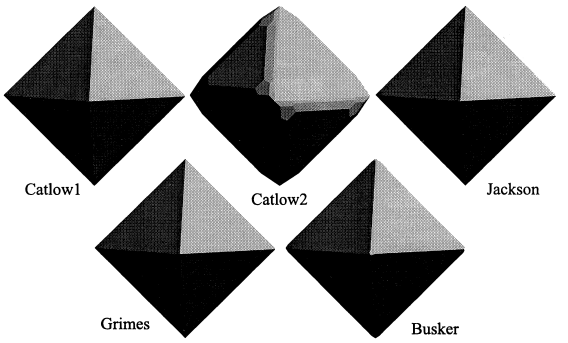

Fig. 4. Equilibrium morphologies of UO_2 for the five applied models.

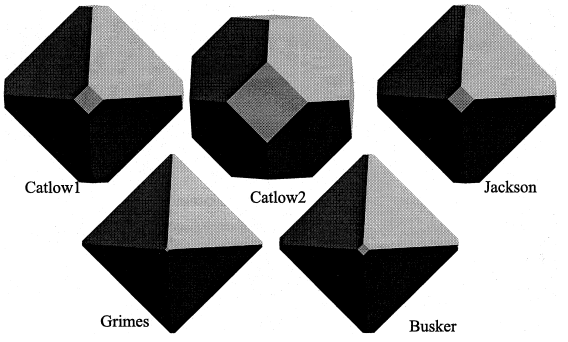

Fig. 5. Growth morphologies of UO_2 for the five applied models.

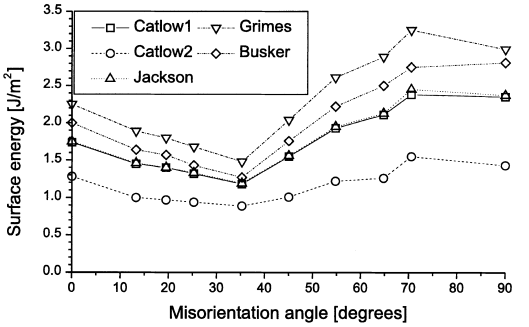

Fig. 6. Surface energy as a function of the misorientation angle for the (1 1 *n*) family of planes.

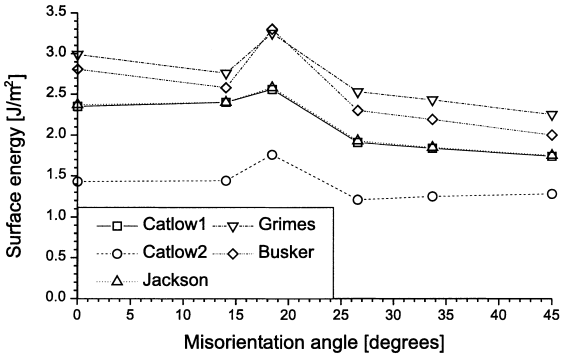

Fig. 7. Surface energy as a function of the misorientation angle for the (0 1 *n*) family of planes.

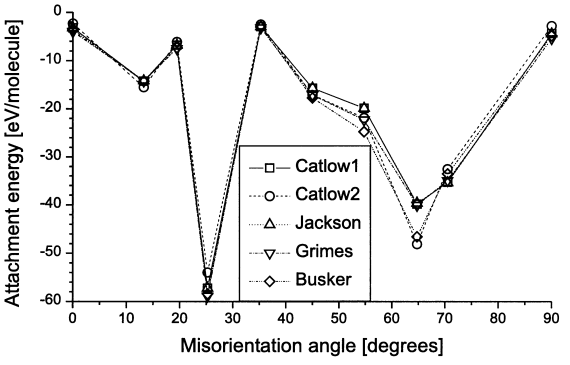

Fig. 8. Attachment energy as a function of the misorientation angle for the (1 1 *n*) family of planes.

attachment energies for the same two sets of planes. Since the (0 1 *n*) set spans from the (0 1 0) to the (0 0 1) plane, only a range of 45° needs to be plotted due to the cubic symmetry of UO_2: the (0 1 *n*) plane is equivalent to the (0 1 1/*n*) plane. It is evident that for each potential model, the variations in surface and attachment energies as a function of misorientation angle are almost the

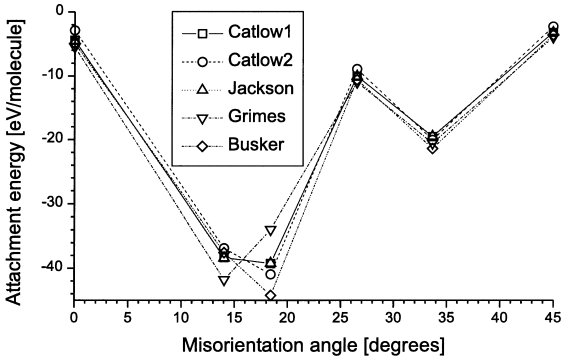

Fig. 9. Attachment energy as a function of the misorientation angle for the (0 1 *n*) family of planes.

same. This includes the Catlow2 model, which employs partial charges and even leads to a modified equilibrium morphology. Therefore, all the calculations of surface and attachment energies for UO_2, despite being based on different interionic potentials, yield a coherent picture, not only with regard to the predicted equilibrium and growth morphologies, but also to the relative energies of many of the surfaces which do not appear in either morphology.

4. Conclusions

The results derived from all five potential models suggest the following: if powder processing conditions are such as to allow the UO_2 crystallites to attain thermodynamic equilibrium, the morphology will be dominated by the (1 1 1) surfaces, forming an octahedron. The tips of these crystallites may possibly be slightly modified by higher order planes, but this effect is expected to be minimal. If thermodynamic equilibrium is not reached and the morphology is limited by growth (i.e. kinetic) considerations, (1 1 1) surfaces are again dominant, but now (2 0 0) surfaces are definitely of some secondary importance, i.e. the morphology will be that of a truncated octahedron.

Of course, we need to bear in mind that the results presented here relate to stoichiometric UO_2. It will therefore be necessary to refine the method so that it is able to predict morphologies of non-stoichiometric materials. In addition, for type III surfaces, the details associated with more complex arrangements of defects need to be further investigated and, if possible, compared to high resolution experimental data.

Furthermore, these conclusions assume that the kiln atmosphere (in particular any water vapour) has no or negligible effect on the developing morphology. Indeed, it is not even clear if in practice a vapour phase formation mechanism is in operation and UO_2 powder may be growing on or from a U_3O_8 substrate. Calculations are under way to investigate the nature of the UO_2:U_3O_8 interface.

Despite these uncertainties, we have been able to demonstrate that it is possible to model UO_2 surfaces, obtain results which are not a function of the particular model and have thereby laid the foundations for further computational studies on UO_2.

Acknowledgements

We are grateful to BNFL (contract A782751), who provide financial support for M.A. Dr A.L. Rohl and Dr D.H. Gay are thanked for supporting our use of their program MARVIN.

References

[1] S.E. Ion, R.H. Watson, E.P. Loch, Nuclear Energy 28 (1989) 21.
[2] G. Harrop, Nuclear Energy 35 (1996) 311.
[3] W.D. Kingery, H.K. Bowen, D.R. Uhlmann, Introduction to Ceramics, Wiley, New York, 1976.
[4] S. Vyas, R.W. Grimes, D.H. Gay, A.L. Rohl, J. Chem. Soc. Faraday Trans. 94 (3) (1998) 427.
[5] M. Castell, C. Muggelberg, Department of Materials, University of Oxford, private communication.
[6] M. Born, Verhandlungen der Deutschen Phys. Gesellschaft (1918) 210.
[7] C.R.A. Catlow, Proc. R. Soc. Lond. A 353 (1977) 533.
[8] R.A. Jackson, C.R.A. Catlow, J. Nucl. Mater. 127 (1985) 161.
[9] R.W. Grimes, C.R.A. Catlow, Philos. Trans. R. Soc. Lond. A 335 (1991) 609.
[10] G. Busker, Imperial College, London, private communication.
[11] D.H. Gay, A.H. Rohl, J. Chem. Soc. Faraday Trans. 91 (1995) 925.
[12] P. Hartman, P. Bennema, J. Cryst. Growth 49 (1980) 145.
[13] G. Springholz, N. Frank, G. Bauer, Appl. Phys. Lett. 64 (1994) 2970.
[14] R.F. Xiao, J. Cryst. Growth 174 (1997) 531.
[15] P.W. Tasker, J. Phys. C 12 (1979) 4977.
[16] G. Wulff, Z. Kristallogr. 34 (1901) 449.